



## ARTICLE

# Moderate Geomagnetic Storm Condition, WAAS Alerts and Real GPS Positioning Quality

Vladislav V. Demyanov<sup>1\*</sup> Xinggong Zhang<sup>2\*</sup> Xiaochun Lu<sup>2</sup>

1 Irkutsk State Transport University, 664074 Chernyshevskogo str.15, Irkutsk, Russia

2 National Time Service Center, Shuyuan east Road 3, Lintong District, Xi'An, China

### ARTICLE INFO

#### Article history

Received: 22 November 2018

Accepted: 7 January 2019

Published: 1 March 2019

#### Keywords:

Ionosphere and SBAS

Auroral oval and WAAS integrity

DGPS

Differential GNSS integrity under geomagnetic storms

### ABSTRACT

The most significant part of Wide Area Augmentation System (WAAS) integrity consists of the User Differential Range Error (UDRE) and the Grid Ionospheric Vertical Error (GIVE). WAAS solutions are not completely appropriate to determine the GIVE term within the entire coverage zone taking in account real irregular structure of the ionosphere. It leads to the larger confidence bounding terms and lower expected positioning availability in comparison to the reality under geomagnetic storm conditions and system outages. Thus a question arises: is the basic WAAS concept appropriate to provide the same efficiency of the integrity monitoring for both “global differential correction” (i.e. clock, ephemeris et al.) and “local differential correction” (i.e. ionosphere, troposphere and multipath)? The aim of this paper is to compare official WAAS integrity monitoring reports and real positioning quality in US coverage zone (CONUS) and Canada area under geomagnetic storm conditions and system outages. In this research we are interested in comparison between real GPS positioning quality based on single-frequency C/A ranging mode and HAL (VAL) values which correspond to the LP, LPV and LPV200 requirements. Significant mismatch of the information between WAAS integrity data and real positioning quality was unfolded as a result of this comparison under geomagnetic storms and system outages on February 14, 2011 and June 22, 2015. Based on this result we think that in order to achieve high confidence of WAAS positioning availability alerts real ionospheric measurements within the wide area coverage zone must be involved instead of the WAAS GIVE values. The better way to realize this idea is to combine WAAS solutions to derive “global differential corrections” and LAAS solutions to derive “local differential corrections”.

## 1. Introduction

The Wide Area Augmentation System (WAAS) provides not only differential corrections, but also ranging error associated confidence bounds to

ensure the integrity of the positioning service throughout the United States and Canada. The WAAS Master Station calculates integrity data associated with its generated corrections at the required level of integrity for the intended flight operation. Integrity data is provided in the form of rang-

\*Corresponding Author:

Vladislav V. Demyanov; Irkutsk State Transport University, 664074 Chernyshevskogo str.15, Irkutsk, Russia

Email: vv.emyanov@gmail.com

Xinggong Zhang; National Time Service Center, Shuyuan east Road 3, Lintong District, Xi'An, China

Email: zyg@ntsc.ac.cn

ing error confident bounds which are broadcast within WAAS coverage zone and is used in order to compute the protection levels (PL) taking into account both all relevant ranging error sources and local “satellite-user” geometry. Depending on the flight operation, the user equipment may either compute a Horizontal Protection Level (HPL) or both a HPL and a Vertical Protection Level (VPL). WAAS guarantees that the user’s actual position error will be smaller than PL values during 99.99999% of the time. The following level accuracy and availability for the WAAS coverage zone has been accepted as:

- 1) Localizer Performance (LP) service is available when the calculated HPL is less than 40 meters;
- 2) Localizer Performance with Vertical Guidance (LPV) service is available when the calculated HPL is less than 40 meters and the VPL is less than 50 meters;
- 3) Localizer Performance with Vertical Guidance to 200 foot decision height (LPV200) service is available when the calculated HPL is less than 40 meters and the VPL is less than 35 meters.

The receiver user compares the computed protection levels with the alert limit (AL) thresholds established for the horizontal plane (HAL) and the vertical plane (VAL) for a selected phase of flight. If one of the protection levels exceeds the corresponding alert limit, the receiver provides an annunciation to the user<sup>[1]</sup>.

The most significant part of the integrity data consists of the User Differential Range Error (UDRE) and the Grid Ionospheric Vertical Error (GIVE). The UDRE characterizes the residual error in the fast and long term “global” corrections of both ephemeris and reference oscillator associated errors. The UDRE is broadcast by the WAAS for each satellite that is monitored by the system and the 99.9% bound (3.29 sigma) of the residual error on a pseudo range after application of fast and long-term corrections is checked. The GIVE characterizes the residual error in the current ionospheric correction (IC), for the estimated ionosphere signal vertical delays are calculated for each of WAAS ionospheric grid point (IGPs) and broadcasted every 5 minutes<sup>[1]</sup>. Since the true ionospheric delay and multipath error are not precisely known, the estimated variants in these error sources are added to the UDRE, before comparing it to the residual error<sup>[2]</sup>.

It is obvious that reliability of WAAS service integrity depends on how the UDRE and GIVE confidence bounds correspond to the real positioning environment. It is well known that current availability of WAAS service strictly depends on both the quality of each individual satellite vehicle (SV) ranging and SVs constellation geometry at the user’s location. Positioning delusion of precision

(PDOP) describes local “satellite-user” geometry and it is unique and unpredictable for each particular user within the WAAS coverage zone. Hence the confidence bounds are established according to the expected UDRE and GIVE values.

For the WAAS, ionospheric ranging errors are the most significant and unpredictable. The horizontal and, especially, the vertical positioning availability are easily to be disturbed in the ionosphere<sup>[3]</sup>. At mid-latitudes such disturbances mostly appear during the main phase of geomagnetic storms and can cause both increasing ranging error and some short outages of GPS SVs<sup>[4,5,6]</sup>. Nevertheless a user derives the GIVE value anywhere in the coverage zone based on the interpolation solutions from the nearest WAAS ionospheric grid points (IGPs) data to compute individual protection levels. In our opinion such a method of the ionospheric signal delays data treatment to get GIVE confidence bounds is not able to deal with undetected multi-scale ionospheric disturbances and yields high probability of false alarm of the HAL (VAL) exceeding. As WAAS solutions are disable to determine the GIVE term within the entire coverage zone taking in to account the real irregular structure of the ionosphere it leads larger confidence bounding terms and lower expected positioning availability in comparison to the reality under geomagnetic storm conditions.

The aim of this paper is to compare official WAAS integrity monitoring reports [[www.nstb.tc.faa.gov/DisplayDailyPlotArchive.htm](http://www.nstb.tc.faa.gov/DisplayDailyPlotArchive.htm)] and real positioning quality in US coverage zone (CONUS) and Canada under geomagnetic storm conditions and system outages. In this paper we are interested in the comparison between real GPS positioning quality based on single-frequency C/A mode and HAL (VAL) values which correspond to the LP, LPV and LPV200 requirements. The aim of such research is to make a first step to answer the question: “Can we use the WAAS typical solutions to provide LPV and LPV200 service outages alerts with required confidence taking in to account the real environment for the future GNSS SBAS?”

## 2. Data Sources and Experimental Environment

We conducted our research under geomagnetic storms condition on February 14-15, 2011 and June 22-23, 2015. Table 1 collects these storms parameters based on geomagnetic data from [<https://cdaweb.sci.gsfc.nasa.gov/>]. The main parameters of geomagnetic storm such as the time of sudden commencement (Tssc), periods of the initial phase (IP), the main phase (MP) and the re-

covering phase (RP) as well as the variations of the horizontal component of the geomagnetic field (Ht) were derived from the high-latitude ground-based magnetometer data at Hampton, Alaska (Lat 64.9, Long 212.1) [https://cdaweb.sci.gsfc.nasa.gov/cgi-bin/eval1.cgi].

Comparison of the above mentioned geomagnetic events displays that the February 14-15, 2015 event has short MP period, weak geomagnetic, hence, ionospheric disturbances and can be considered as a moderate geomagnetic storm. In contrast to that the June 22-23, 2015 event is a strong geomagnetic storm which has a long MP period and should be accompanied with significant ionospheric disturbances and can bring significant impact on WAAS and GNSS performance.

**Table 1.** The geomagnetic storms characteristics

Date (yy-mm-dd)	3-hour Kpmax	TSSC, UTC	IP period	MP period	RP period	Htmin, nT	Htmin - Htmax, nT
2011-02-14	4	16.00	16.00-20.30	20.30-23.30	After 23.30	12420	12420-12830
2015-06-22	8	05.30	05.30-12.30	12.30-20.00	After 20.00	11500	11500-13000

Usually weak geomagnetic storm is unlikely to induce strong ionospheric disturbances into the mid-latitudes ionosphere. As it was found earlier [7] the multi-scale ionospheric disturbances propagates toward the mid-latitudes from the expanding south boarder of the auroral oval which is considered as a source of acoustic-gravity waves. The area of the auroral oval boarder expands as the further the stronger geomagnetic storm is. So it is unlikely that a weak geomagnetic storm on February 14-15, 2011 is able to inspire strong travelling ionospheric disturbances toward the mid-latitudes. There for the real ionosphere shall not be significantly disturbed in mid-latitudes and the expected WAAS area coverage zone should not shrink as a result of the ionospheric disturbances than.

On the other hand, strong geomagnetic storm, like the event on June 22-23, 2015, can bring serious WAAS performance deterioration. Thus it would be interesting to compare the official WAAS alerts and real GPS positioning quality under both weak and strong geomagnetic storm conditions. That was the reason why we choose the above mentioned days for our research in this paper.

The WAAS official data source [http://www.nstb.tc.faa.gov/DisplayDailyPlotArchive.htm] issued alert reports for the CONUS zone. Fig. 1 a,b displays percent of CONUS area covered with LP, LPV and LPV2000 services versus Greenwech Mean Time (GMT) time on February14 (panel b) and 15 (panel a), 2011.

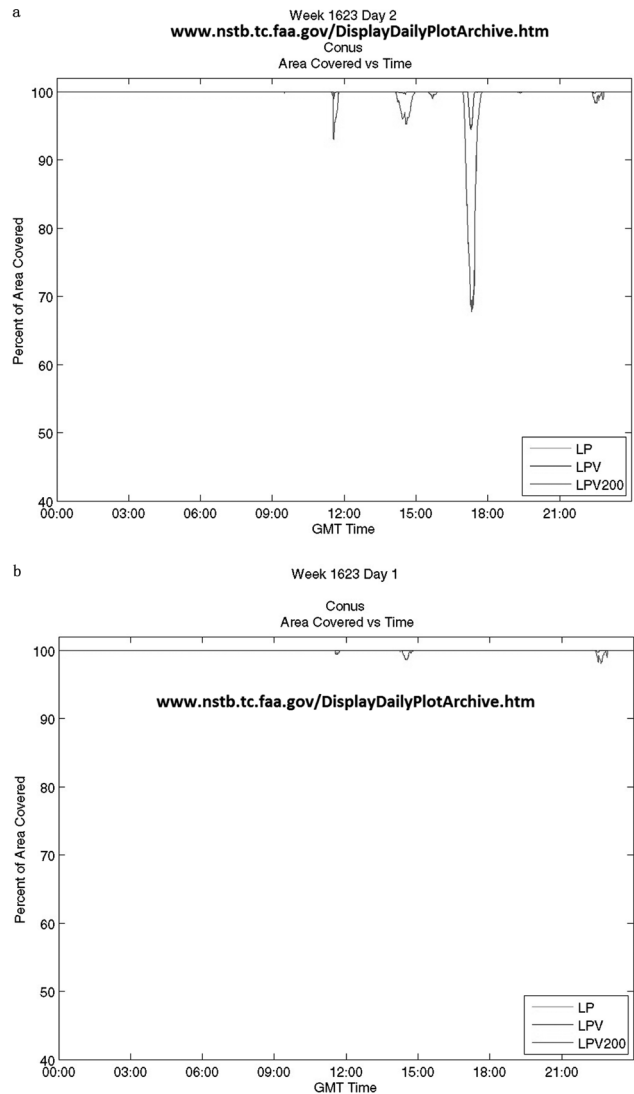


**Figure 1.** Percent of CONUS area covered vs GMT for the day of the main phase of geomagnetic storm on Feb.14, 2011(panel b) and for the day of recovering phase of the geomagnetic storm on Feb 15, 2011 (panel a)

Regardless the main phase of the geomagnetic storm that took place on February14, 2011, we can see that there is no significant coverage zone shrinking for LP, LPV and LPV200 service on this day. However we have WAAS alert of sharp shrinking of the coverage zone at about 17.40 GMT on February 15, 2011 for LPV200 service. This time period corresponds to the end of the recovering phase of the geomagnetic storm. Thereby the ionospheric disturbances are not the probable source of the WAAS coverage zone shrinking here.

Figure 2 displays daily WAAS CONUS LPV and LPV200 coverage versus date and daily Kp indices for a period from January 1st till April 1st 2011 [8]. One can see that sharp shrinking of the WAAS CONUS coverage zone for LPV and LPV200 took place on February 15, 2011 as

well. WAAS CONUS LPV and LPV200 percent of area covered is reduced down to 89% and 73% correspondently.

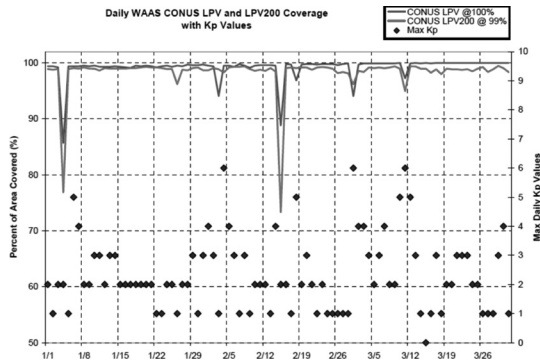


**Figure 2.** Daily percent of CONUS WAAS area coverage and Kp values versus time<sup>[8]</sup>

The WAAS service degradation can be caused by not only the ionosphere impact but also by the WAAS and GPS segments outages. Table 2 contains a list of the system outages which took place on February 14 and 15 2011<sup>[8]</sup>. According to the Table there was GEO Uplink Subsystem (GUS) event for the geostationary satellite GEO138 on February 14, 2011. This event did not cause the LPV and LPV200 outages on this day thanks to the other GEOs, which were used to broadcast WAAS corrections.

There was a long outage for GPS SV PRN 21 (from 11.15 till 20.05 GMT) and short outage for GPS SV PRN 4 (from 11.32 till 11.43 GMT). It means that there were two GPS SV out of service within the period from 11.32 till 11.43 concurrently. These events do not have time coincidence with the WAAS alert picture (Fig. 1) for whole CONUS zone, but according to the WAAS forecast these outages brought LPV and LPV200 service outage in California, the USA North-Central, Arizona and Florida on February 15, 2011.

Fig. 3 a,b displays percent of Canadian area covered with LP, LPV and LPV2000 services vs GMT on June 20 (panel a) and June 22 (panel b), 2015 [http://www.nstb.

tc.faa.gov/DisplayDailyPlotArchive.htm].

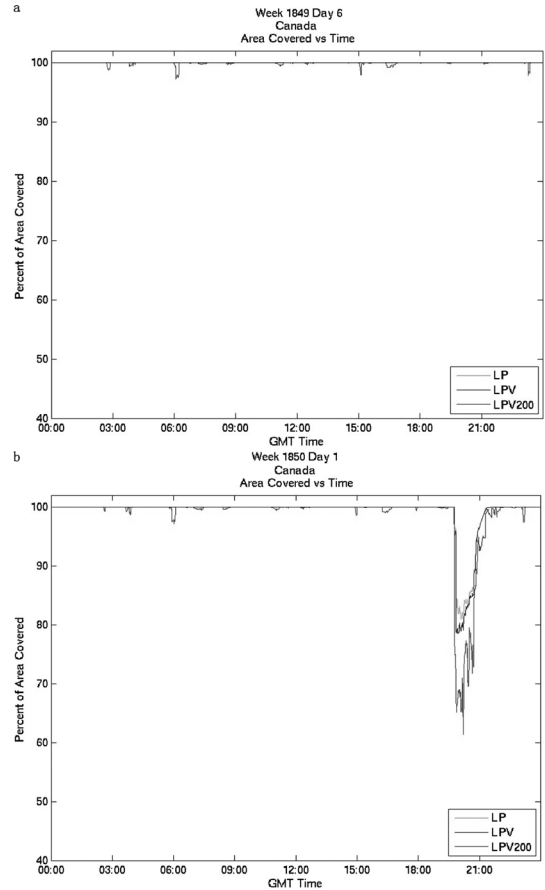


**Figure 3.** Percent of Canadian area covered vs GMT for the day of the geomagnetic storm on June 22, 2015 (panel b) and for the background day on June 20, 2015 (panel a)

Based on the Fig 3, we can see that there was significant degradation of all the LP, LPV and LPV-200 services coverage in Canada from about 19:30 GMT till 21:30 GMT on June 22nd. This time period corresponds to the main phase of strong geomagnetic storm (see Table 1). Fig 4 displays an apparent time coincidence between high Kp=8 and sharp deterioration of LPV and LPV200 services coverage in Canada on June 22, 2015 as well<sup>[9]</sup>.

**Table 2.** WAAS and GPS events on February 14 and 15, 2011

Start Date	End Date	Location/ Satellite	Service Affected	Event Description
02/14/11	02/14/11	GEO138, Woodbine (QWE)	All	GUS switchover, Woodbine faulted. TOW 127889-127902
02/15/11	02/15/11	PRN21	All	NANU 2011015. There was a NANU 2011015 on PRN 21 from 11:15am to 20:05pm GMT and SV Alert on PRN 4 (11:32am-11:43am), which both affected LPV and LPV200 coverage; W1623D2 LPV Outages: 1. California outage due to SV alert on PRN 4; 2. North-Central and Arizona outages due to NANU on PRN 21 LPV200 Outages: 1. California outage due to SV alert on PRN 4; 2. North-Central, Arizona and Florida outages due to NANU on PRN 21;

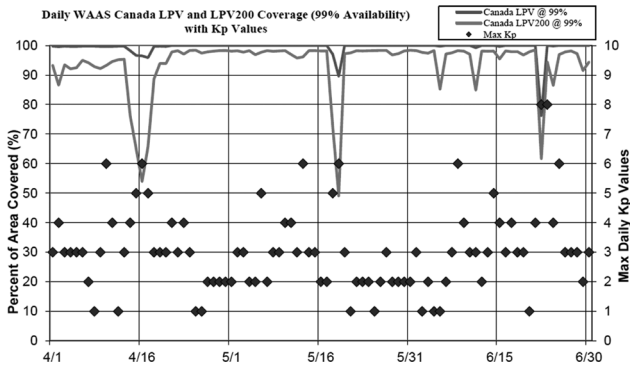


**Figure 4.** Daily percent of Canada LPV and LPV200 service area coverage and Kp values versus time

Table 3 contents the LPV (LPV200) service degradation event description. In contrast to the previous case (see Table 2) the service degradation for all the North America coverage zone is caused by the ionospheric disturbances as a result of strong geomagnetic storm on June 22-23, 2015 [9].

According to Table 3 there were no GPS/WAAS segment outages during the event on June 22, 2015 so we can be sure that the LPV and LPV200 service degradation was caused with elevated GIVE values as a result of the ionospheric geomagnetic disturbances. As all the events took place during the MP and the beginning of the RP of the geomagnetic storm we can probably consider the LPV and the LPV200 service degradation as a result of the travelling ionospheric disturbances from the pulsing auroral oval border [7].

### 3. Data Sources and Data Treatment

To compare the WAAS alerts to the real positioning quality we utilized RINEX 2.0 data files with 30-s time resolution which are available on [http://lox.ucsd.edu/pub/rinex/]. These data corresponds to GPS-sites which are placed in CONUS and Canada zones. For our research goals 70 sites in CONUS zone (excluding California) and

30 sites in Canada were chosen. The CONUS sites were equipped with the same GPS receiver type Trimble in order to avoid influence of the apparatus features of different GPS receiver type to our final results. Unfortunately there were not enough sites equipped with the same type of receivers in Canada. These Canadian sites were equipped with different types of receivers such as TPS Net, Leica, Ashtech, Trimble, AOA and Turbo-Rogue. The map of these sites location for both CONUS and Canada zones is displayed in Fig.5.

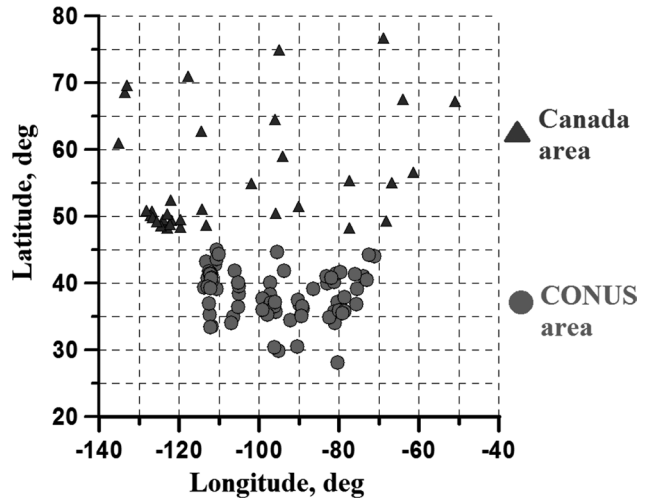


**Figure 5.** A map of the GPS-sites location within CONUS and Canada zone coverage zone

Firstly, it is interesting to compare the WAAS alert figures (Fig1-4) and the real positioning quality in CONUS and Canada coverage zone. In order to do this a percent of area coverage with the real positioning service for CONUS and Canada zones was derived, based on the RINEX data for each of GPS-sites (Fig 5) in one-frequency with the GPS standalone mode. TEQC software [10] was utilized to get navigation solutions and the correspondent positioning errors for the GPS-sites. Doing this, we did not use the ionospheric correction and GPS SV outages report (Table 2) in order to simulate that GPS standalone mode which

**Table 3.** WAAS and GPS events on June 22, 2015

Start Date	End Date	Location/ Satellite	Service Affected	Event Description
2016/06/22	2016/06/23	Washington D.C. (CnV), Los Angeles (CnV), Atlanta (CnV)	LPV_All, LPV200_All,	Geomagnetic activity (Kp = 8 ) disturbed the ionosphere causing elevated GIVE values. This resulted in significant degradation of: (1) LPV-200 service coverage in Canada from about 19:45 GMT until 21:35 GMT on June 22nd. The elevated GIVE values also resulted in moderate degradation of: (1) LPV service coverage in Canada from about 19:45 to 21:16 GMT on June 22nd; (2) LPV-200 service coverage in CONUS (Northeast) from about 19:45 to 21:07 GMT on June 22nd. The elevated GIVE values also resulted in minor degradation of: (1) LPV service coverage in CONUS (Northeast) from about 19:45 to 20:45 GMT on June 22nd and LPV-200 service coverage in Alaska from about 20:16 to 20:26 GMT on June 22nd

corresponds to the worst case of positioning conditions.

In case of mismatch of alert figures from the WAAS output and TEQC output we need to involve another independent solution for HPL (VAL) computation to decide which alert corresponds to the real environment better. In order to do it, we compute HPL (VAL) values based on the real ionospheric ranging error statistics, instead of GIVE values for each GPS site within CONUS and Canada zones. Taking all of this in to account, our strategy of the data treatment includes following steps:

1) Getting the navigation solutions with 30-s time resolution for each GPS site (Fig.5) utilizing RINEX within one-frequency C/A ranging data and TEQC software. Once the navigation solution had been received we computed the positioning errors of each GPS site and transform the error values from rectangular Earth-centered coordinate system to the local coordinate system;

2) Comparison between the LP, LPV and LPV200 alarm limits (HAL and VAL) and real positioning errors which were computed at the pervious step. Every time when positioning error exceeds correspondent alarm limit a positioning fault is fixed for the GPS site according to LP, LPV or LPV200 limits particularly. Finally the real percent of the area covered for CONUS or Canada zone is computed as following:

$$\% \text{ of Area covered} = \frac{(N_{TOT} - N_{FLT})}{N_{TOT}} \cdot 100\% \quad (1)$$

Where  $N_{TOT}$  is total amount of GPS-sites within the area under consideration;  $N_{FLT}$  is the number of the GPS-sites where the current positioning errors exceed either the VAL or HAL values according to the LP, LPV or LPV200 services.

3) A computation current HPL and VPL values taking in to account the real ionospheric ranging errors instead of correspondent GIVE values. In order to do this, a “model ranging” and real SVs constellation were utilized for each GPS-site within the CONUS or Canada zone. Here we define “model ranging” as following:

$$\begin{aligned} \rho_i &= R_{GEOM,i} + \Delta R_{ion,i} \\ R_{GEOM,i} &= \sqrt{(x_{0,i} - x_{US})^2 + (y_{0,i} - y_{US})^2 + (z_{0,i} - z_{US})^2} \\ \Delta R_{ion,i} &= \frac{40.308}{f_1^2} \cdot TEC_i \\ TEC_i &= \frac{1}{40.308} \cdot \frac{f_1^2 \cdot f_2^2}{f_1^2 - f_2^2} \cdot (C1_i - P2_i) \end{aligned} \quad (2)$$

Where:  $x_{0,i}, y_{0,i}, z_{0,i}$  and  $x_{US}, y_{US}, z_{US}$  are  $i$ -th SV position and user’s position in the rectangular Earth-centered coordinate system. These data can be found or computed from the correspondent RINEX files;  $TEC_i$  is ionospheric

total electron content along the “ $i$ -th SV-user” line-of-site (in TECU,  $1TECU=10^{16} \text{ 1/m}^2$ );  $f_1=1575.25 \text{ GHz}$  and  $f_2=1227.75 \text{ GHz}$  are the GPS operation frequencies;  $C1_i$  is C/A-code ranging at frequency  $f_1$  and  $P2_i$  is P-code ranging at frequency  $f_2$  which can be derived from RINEX observation file for each SV in view.

Computation of the HPL and VPL protection levels for a “model ranging” (2) and the real SVs constellation for each of the GPS-sites can be done as following<sup>[11]</sup>

$$\begin{aligned} HPL &= \begin{cases} K_{HNPA} \cdot D_{mjr} \\ \text{or} \\ K_{HPA} \cdot D_{mjr} \end{cases} ; \quad VPL = K_{VPA} \cdot D_V \\ D_{mjr} &= \sqrt{\frac{D_X^2 + D_Y^2}{2} + \sqrt{\left(\frac{D_X^2 - D_Y^2}{2}\right)^2 + D_{XY}^2}} \\ D_X^2 &= \sum_{i=1}^N S_{X,i}^2 \cdot \sigma_i^2 ; \quad D_Y^2 = \sum_{i=1}^N S_{Y,i}^2 \cdot \sigma_i^2 ; \quad D_V^2 = \sum_{i=1}^N S_{V,i}^2 \cdot \sigma_i^2 \\ D_{XY} &= \sum_{i=1}^N S_{X,i} \cdot S_{Y,i} \cdot \sigma_i^2 \\ \mathbf{S} &= \begin{bmatrix} S_{X,1} & S_{X,2} & \dots & S_{X,N} \\ S_{Y,1} & S_{Y,2} & \dots & S_{Y,N} \\ S_{V,1} & S_{V,2} & \dots & S_{V,N} \\ S_{t,1} & S_{t,2} & \dots & S_{t,N} \end{bmatrix} = (\mathbf{G}^T \cdot \mathbf{W} \cdot \mathbf{G})^{-1} \cdot \mathbf{G}^T \cdot \mathbf{W} \end{aligned} \quad (3)$$

Where  $K_{HNPA}=6.18$  is a coefficient of confidence bounds in horizontal plane for non-precise landing approaching;  $K_{HPA}=6.0$  is a coefficient of confidence bounds in horizontal plane for precise landing approaching with vertical guidance;  $K_{VPA}=5.33$  is a coefficient of confidence bounds in vertical plane for a precise landing approach with vertical guidance;  $\mathbf{G}$  is current “SV-user” angular geometry matrix;  $\mathbf{W}$  is diagonal ranging errors weighting matrix;  $\sigma_i$  is a standard deviation of the “model ranging” error (2) for  $i$ -th SV.

As we need to find  $\sigma_i$  – values for each SV in the view before the HPL and VPL computation it means that we have to accumulate simultaneous ranging values within some time interval. The time interval of  $\Delta T=5 \text{ min}$  was used in our computation here.

4) A comparison between the current HPL and VPL values (3) and correspondent alarm levels of LP, LPV and LPV200 services for each GPS-site from CONUS or Canada areas and the percent of area covered computation (1) than.

To model the ranging time series (2) based on the real data from the correspondent RINEX files the double-frequency P1 (or C1) - P2 “code-code” combination was utilized. It means that the current  $\Delta R_{ion,i}$  value (2) contents not only the pure ionospheric signal delays but also the residuals of all the frequency dependent ranging errors, such as multipath error and differential code biases (DCB)

in SV and the receiver equipment.

In order to understand the final results clearly we should evaluate expected ranging errors before getting navigation solution from the “model ranging” data. Based on a long time research it has been accepted that the most probable value of the vertical user ionospheric range error (UIRE) can be assumed in the WAAS solutions as follows [11]

$$\Delta R_{UIRE,V} = \begin{cases} 9.0\text{ m} & 0^\circ \leq \phi_{PP} \leq 20^\circ \\ 4.5\text{ m} & 20^\circ < \phi_{PP} \leq 55^\circ \\ 6.0\text{ m} & 55^\circ < \phi_{PP} \end{cases} \quad (4)$$

Where  $\phi_{PP}$  is the latitude of the ionospheric pierce point.

To transform this vertical range error into the correspondent slant error value we can use following equation [12]

$$\Delta R_{UIRE,SLT} = \Delta R_{UIRE,V} \cdot \left( 1 - \left( \frac{R_E \cos(ELE)}{R_E + h_{F2}} \right)^2 \right)^{-0.5} \quad (5)$$

Where  $R_E = 6378.1363$  km is the Earth radius;  $h_{F2} = 350$  km is the height of the F2 layer electronic density maximum concentration; ELE is a SV elevation angle.

Based on the IGS statistics of the expected ionospheric TEC grid forecasting the 1-sigma confidence bounds of this parameter should be within 2-9 TECU (correspondent UIRE is from 0.32 to 1.44 m).

The absolute value of standard mean of the SV DCB shall not exceed 15 ns (4.5 m). The main DCB can be either positive or negative. The random variations of this value shall not exceed 3 ns i.e. 0.9 m (two sigma). In a reality SV DCB differs significantly for different types of SV and can vary within +/- 12 ns (i.e. +/- 3.6 m) from one SV to another. SV DCB value has a long lasting trend changing as much as 0.3-0.5 ns per year [13,14].

DCB values for the GPS receiver strictly depends on the receiver type and environment condition. According to [14] it was found that, the absolute value of receiver DCB can vary within +/- 40 ns (i.e +/- 12 m) for the Trimble 5700 and Trimble NETP types. The random variations of this value (1-sigma) shall not exceed 2 ns (0.6 m). Like the previous item, the mean of this code delay can be either positive or negative and have the long annual trend.

There are many evaluations of multiphase effects on the GNSS performance [15,16]. This error is usually considered as zero-mean Gaussian noise with standard deviation which depends on the SV elevation angle as following [11].

$$\sigma_{MPH} = 0.13 + 0.53 \cdot \exp\left(\frac{-ELE_i}{10^\circ}\right) \quad (6)$$

Based on (6) the one-sigma confidence bound of multipath error standard deviation is within 0.13 – 0.4 m depending on the SV elevation angle.

Taking into account all the above mentioned components we can expect that standard mean of the  $\Delta R_{ion,i}$  values (2) which were derived from the RINEX (P1(C1)-P2) data is expected to be from -3.2 to 28 m and correspondent standard deviation is from 0.8 to 4.2 m. Figure 6 displays daily values of standard mean and standard deviation of  $\Delta R_{ion,i}$  values which were derived from RINEX data utilizing (2) for each GPS-site in CONUS area. One can see that all these values are within the previously computed borders. There is no significant difference between these data on February 14 and 15, 2011. Figure 7 displays the same data which were derived from RINEX data for each GPS-site in Canada.

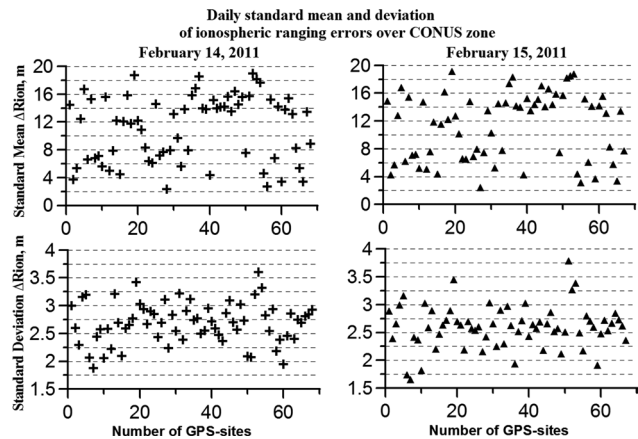


**Figure 6.** Daily Standard Mean and Standard Deviation of the ionospheric ranging errors derived from the RINEX data corresponding to the GPS sites which are within CONUS zone on February 14 (left panel) and February 15 (right panel), 2011

Two groups of the daily standard mean of  $\Delta R_{ion,i}$  values can be recognized in Fig 6 according to their values. First group of the standard mean values lies within 10-20 meters but another group is within 2-10 m. This difference probably can be explained with different type of antennas and GPS receivers which are set on different GPS-sites under our consideration. On the other hand there is no such a significant difference between standard deviation values which were taken from the same data series. All the values vary within the 1.5-3.7 m on both February 14 and 15, 2011.

Regardless the Canadian GPS-network contain the GPS receivers of several types, similar features of the daily standard mean and standard deviation can be seen in

Fig.7. Most of the daily standard mean of  $\Delta R_{ion,i}$  values lie within 2-10 m. On the other hand a bit higher standard deviation values can be seen here. All the values vary within the 1.6-4.2 m on both June 20th and 22nd, 2015.

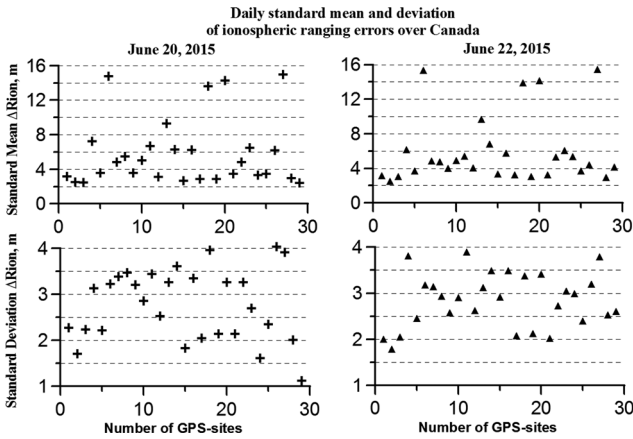


**Figure 7.** Daily Standard Mean and Standard Deviation of the ionospheric ranging errors derived from the RINEX data corresponding to the GPS sites which are within Canada on June 20th (left panel) and June 22nd (right panel), 2015

### 3.1 Real Positioning Quality and WAAS Alerts Comparison

Positioning quality is considered at the standpoint of the protection cylinder concept<sup>[1]</sup>. This protection cylinder, is centered on the user’s calculated position and represents the uncertainty of the position according to user’s true position at each time point. In our research the data from the GPS-sites with constant position is used. Thus user’s true position can be considered as known. On the other hand the alert limit cylinder is utilized to check if the current positioning accuracy corresponds to LP, LPV or LPV200 required positioning accuracy. The alert limit cylinder is centered on the user’s calculated position, just as the protection level cylinder, and defined with the HAL and VAL borders. In case if the user’s calculated positioning errors exceeds either the VAL or HAL values, it means that required positioning accuracy is not available.

The percent of area covered (1) was computed for the LP, LPV and LPV200 alert limits particularly. To evaluate positioning quality from TEQC output data we did not use any ionospheric correction in order to pure the prob-able ionospheric impact better. Fig.8 displays the percent of CONUS area covered versus UT. Can be seen that the percent of area covered was not decreasing lower than 82% for all protection limits neither on February 14th (the main phase of geomagnetic storm) nor on February 15th (recovering phase of geomagnetic storm).

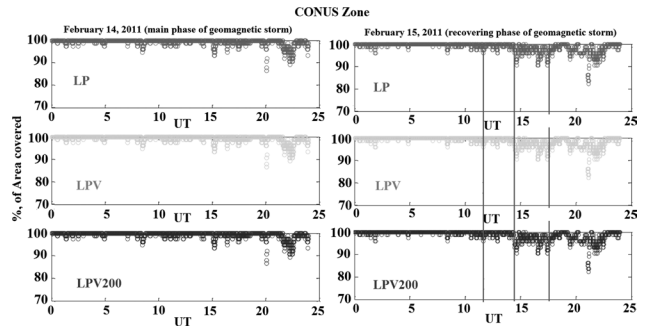


**Figure 8.** TEQC output: percent of CONUS area covered vs Time on Feb. 14 (left panel) and on Feb. 15 (right panel), 2011. Red lines mark approximate time points which correspond to WAAS alerts (see Fig 1a).

Comparison between these results and the WAAS official alerts (Fig.1,2) displays following:

1) TEQC output data analysis displays that positioning quality is worse within the time period from 15.00 to 23.00 UT on February 15 in comparison to the same time on the previous day. This time period corresponds to the end of recovering phase of the geomagnetic storm (Table 1). Hence the percent of area coverage shrinking is not likely caused with the ionospheric geomagnetic disturbances in this time period. According to Table 2, there was a long SV PRN 21 outage from 11.15 till 20.05 UT, so it can be considered as a probable source of positioning quality deterioration within CONUS coverage zone in the period before 20.05 UT.

2) There are two apparent periods of the CONUS area covered shrinking on February 15th, 2011. The first period lasts from 14.30 to 18.00 UT and generally coincides with the WAAS alerts (Fig.1 a). But according to the TEQC output data the real positioning quality is worse within the second period from 19.30 to 22.00 in comparison to the period from 14.30 to 18.00 UT. However WAAS does not provide any alerts for this second period of positioning quality decreasing;

3) WAAS alerts displays the lowest percent of the CONUS area covered which is less than 70% at 17.40 UT for LPV200 service (Fig.1 a). This value is much lower in comparison to the correspondent TEQC output results with is about 90% at the same time point (Fig. 8, right panel). We can consider such a mismatch as probable false alarm event in WAAS output.

4) There are certain events of the positioning quality deterioration at 09.00-09.30 UT, at about 15.00 UT and at about 20.00 UT for both Feb.14th and 15th, 2011. As these events take place on both days and at the same time points they probably have nothing to do with ionospheric disturbances. These events can be probably caused by such regular events as “local spots of bad visibility” of the

GPS SV constellation. Such events can bring periodic regular variations of the local PDOP values which can repeat and move in local areas.

Generally there is a significant mismatch between TEQC output data and the WAAS alerts figure on both February 14 and 15 2011. It can be explained as we did not use any ranging corrections and we get the lower percent of the area covered in comparison to the WAAS alert figure. Some cases, however, can be considered as probable WAAS output mismatch information or false alarm but in order to prove it we need to crosscheck the data involving additional independent means of positioning availability control.

Fig.9 displays the percent of Canada area covered versus UT. We can see that the percent of area covered was not decreasing lower than 80% for all protection limits neither on June 20th (background day) no on June 22nd (initial and main phases of the geomagnetic storm).

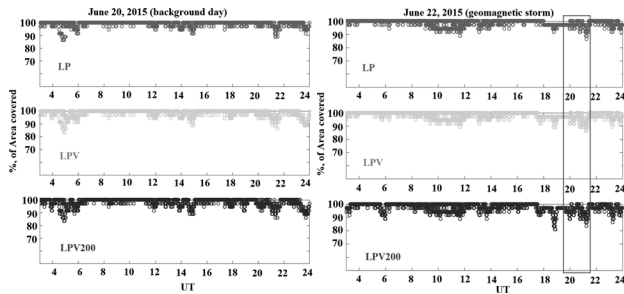


**Figure 9.** TEQC output: percent of the Canada area covered vs the UT on June 20<sup>th</sup> (left panel) and on June 22<sup>nd</sup> (right panel), 2015. The red rectangle marks the time period which corresponds to the WAAS alerts (see Fig 3b)

In contrast to the previous case the WAAS official alert gives significant percent of area covered shrinking which is expected from 19.45 to 21.35 UT on June 22, 2015 as a consequence of the strong geomagnetic storm (see Table 3). On the other hand there were not cases of the system outages on June 22<sup>nd</sup>, thereby the positioning deterioration events can be certainly considered as consequence of the ionospheric geomagnetic disturbances. According to Fig 9 we can find following results:

1) TEQC output data displays that positioning quality is generally worse on June 22<sup>nd</sup>, 2015 in comparison to the previous geomagnetically quiet day. It is especially true for the time period from 17.30 to 22.00 UT on June 22<sup>nd</sup> (Fig. 9, right panel). This time period partially coincides with the WAAS alert (Table 3) but TEQC output data gets 85% of the lowest % of area covered that is in 20% higher in comparison with the WAAS alert data (Fig.3b).

2) Like the previous case there are certain events of the positioning quality deterioration at 05.00 UT, at about 14.00 UT, at about 21.30 UT and at 23.30 UT for both

June 20 and 22, 2015. As these events take place on both days and at the same time periods they can probably be explained with the regular variations of the local PDOP values like previously.

3) There is a period of significant shrinking of the % of area covered at about 05.00 to 05.30 UT on June 20, 2015 (Fig 9, left panel). It was a background geomagnetically quiet day so this event has nothing to do with the geomagnetic storm impact. However, we should note that the most part of Canada is within the auroral oval area even under the geomagnetic quiet days. Such environment can bring ionospheric disturbances and GNSS signal quality deterioration even under a geomagnetically quiet condition [7].

Generally both TEQC output data and the WAAS alerts figure display an obvious shrinking of the % of area covered in Canada area on June 22<sup>nd</sup>, 2015 in the time period from about 09.00 to 22.00 UT under geomagnetic storm condition. This time period mostly corresponds to the main phase of the storm. Regardless we did not use any ionospheric correction the lowest % of area covered for the TEQC output data is in 20% higher in comparison with the WAAS alert figure. It can be considered as probable mismatch information or false alarm at the WAAS output.

### 3.2 Model Protection Levels and WAAS Alerts Comparison

A comparison between the previous results and the results of “model” protection levels computation based on (2) and (3) was conducted. Fig.10 displays the percent of CONUS area covered versus UT as a result of HPL (VPL) model computation. As it was defined in the previous section the time resolution of HPL and VPL computation was 5 minute. This time period corresponds to the period of the GIVE values computation in a real WAAS [11].

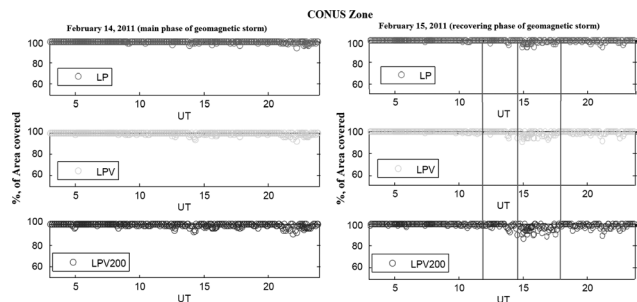


**Figure 10.** Modeling results: percent of CONUS area covered vs Time on Feb. 14<sup>th</sup> (left panel) and on Feb. 15<sup>th</sup> (right panel), 2011. Red lines mark approximate time points which correspond to WAAS alerts (see Fig 1 a).

Comparison between Fig.10 (left panel) and the WAAS alert figure on February 14<sup>th</sup> (Fig 1, b) displays general

accordance, especially for LPV200 service. According to the modeling results the lowest percent of area covered was about 93% for the LPV200 at 22.00-22.30 UT. It was expected that this value should be lower in comparison with the correspondent WAAS LPV200 alert figure on February 14<sup>th</sup>, 2011 (Fig.1 a), because we did not use any ionospheric correction in model computation (2).

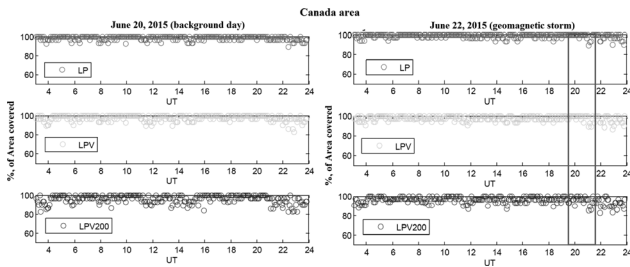


**Figure 11.** Modeling results: percent of Canada area covered vs Time on June 20th (left panel) and on June 22nd (right panel), 2015. The red rectangle marks the time period which corresponds to the WAAS alerts (see Fig 3 b).

The HPL (VPL) modeling computation displays lower % of the CONUS area covered on February 15th, 2011 in comparison to the previous day. The events of the lowest % of area covered takes place in the time period from 14.00 to 18.00 UT (Fig. 10, right panel) which is generally coincides with the WAAS alert figure (Fig.1 a). Nevertheless the lowest percent of the area covered was 85% at about 15.00 UT for the model computation which is in 8-10% less in comparison with the WAAS alert figure for the same time. On the other hand the LPV200 modelling computation gets about 95% of the area covered at 17.30 UT which is in 30% higher in comparison with the WAAS alert for the same time point (Fig.1 a). As the modelling results gets similar figure to the TEQC output data we can suppose that such mismatch of alert figures between the WAAS data and our modeling results displays probable WAAS false alarm in protection levels computation in this time period.

Fig.11 displays the percent of Canada area covered versus UT as a result of the HPL (VPL) model computation. In contrast to the previous case this modelling computation displays obvious accordance neither the WAAS alert figure (Fig.3) nor the real positioning quality figure (Fig.9). Generally we can see random character of the model LP (LPV) computation results but there are events of the % of the area covered decreasing at about 04.00 UT, 12.00 UT and 23.00 UT on both June 20th and June 22nd, 2015. Probably it can be explained with periodic regular variations of the local PDOP values in the same local areas.

There is no obvious decreasing in percent of the Canada area covered within the time period from 19.30 to 21.30 UT on June 22, 2015, so there is no accordance

between the modelling results and the WAAS alert figure this time. There is no significant difference between the modeling computation results for June 20th and June 22nd, 2015 data in Fig 11. However the lowest value of the % of the Canada area covered was not lower than 80 % for all protection levels on both days of the observation. For the LPV 200 protection level this value is in 15-20% higher comparing to the WAAS alert figure (Fig.3 b). Therefore we see probable mismatch of alert figures between the WAAS data and our modeling results in above mentioned environment again.

#### 4. Discussion and Conclusion

Firstly, we should point out the random character of the modelling computation results on June 20-22<sup>nd</sup>, 2015 again(Fig 11). One of the probable explanations can be that there was the lack of GPS- sites we used to compute protection levels in Canada area. On the other hand there is a big difference between radio propagation media in ionosphere above the CONUS and the Canada areas.

Fig 12a displays the position of the south border of the auroral oval versus the UT on June 20th (solid green line) and on June 22nd, 2015 (dashed red line). This figure was derived based on the geophysical data (<https://iswa.gsfc.nasa.gov/IswaSystemWebApp/>). According to the figure we can see that most of the Canada is within the auroral oval on both geomagnetically quiet and, especially, stormy days. It drives us to think that most of the GPS SV line-of-sight pass through high-latitude ionosphere which always contains multi-scale ionospheric irregularities in contrast to the mid-latitude ionosphere (i.e. above the CONUS zone). The main conclusion rises that we may not use the same solution and the same data set of WAAS reference stations (WRS) to reconstruct the ionospheric GIVE values in the same manner for both Canada and CONUS areas.

There is no obvious accordance in time behavior between the modeled LP (LPV) time series (Fig. 11, right panel), dynamics of the ovation prime energy flux of electrons and ions (Fig.12 b) and dynamics of the auroral oval south border(Fig 12a). On the other hand a coincidence in time can be noticed between the WAAS alert (Fig.2 b) and peak of the ovation prime energy flux of electrons and ions at 20.00 UT (Fig.12 b). It is interesting result which displays a contradiction between the real positioning quality and expected protection levels based on the model representations of the GIVE values.

Regardless the peak of the ovation prime energy flux took place at 20.00 UT the most part of the flux energy fell on the North Atlantic, Europe and North of Russia that

time. Indeed we can see that this energy flux did not bring significant motion in the south border of the auroral oval in the North America (Fig.12a). On the other hand the first lower peak of the ovation prime energy flux at 07.00 UT (Fig.12b) mostly falls on the North America and inspired significant shifting in the auroral oval border toward the south. However it did not bring noticeable features in both WAAS alert figure and real positioning quality results.

Our results display some cases of significant mismatch between the WAAS alert figure and real positioning quality for both the CONUS zone and Canada. This mismatch was proved by means of the model computation of HPL (VPL) values based on the real ionospheric ranging errors which were derived from the GPS sites within CONUS zone and Canada. The WAAS alerts got the expected percent of area covered which is much lower in comparison to the real positioning data for both the GPS standalone mode and the model HPL (VPL) computation in the most cases under consideration.

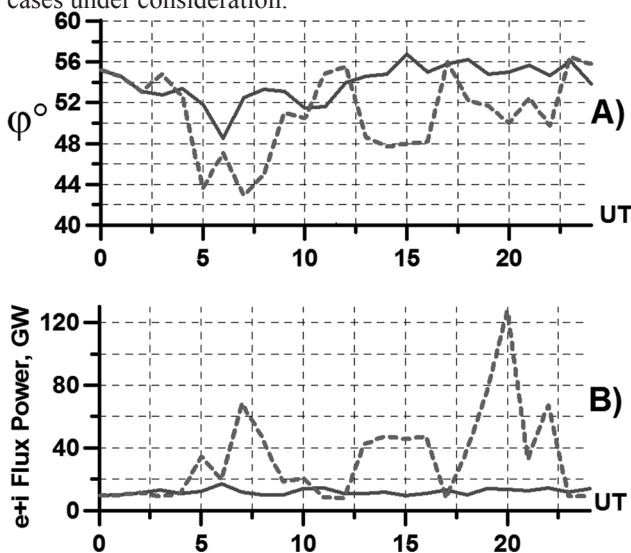


**Figure 12.** South border of the auroral oval dynamics and solar particles energy: panel a) position of the south border of the auroral oval vs time on June 20th (solid green line) and on June 22nd, 2015 (dashed red line); panel b) ovation prime energy flux (electrons+ ions precipitation within aurora) vs time on June 20th (solid green line) and on June 22nd, 2015 (dashed red line).

As it was shown the WAAS integrity service provides general response on the geomagnetic storm. Some particular cases, however, can be considered as probable false alarm of the HAL (VAL) exceeding. Indeed the WAAS alert figure gives much lower expected positioning availability under the geomagnetic storm conditions in comparison to our results at 17.40 UT on February 15th, 2011 and at 19.45-21.35 UT on June 22nd, 2015. In the first case, the real positioning quality according to the LPV

and LPV200 requirements is provided more than 90 % percent of the CONUS area covered. This value is much higher comparing to the correspondent WAAS report (less than 70%) for the same conditions. Model HPL and VPL computation based on the real ionospheric ranging errors get the lowest percent of the area covered which is about 93% for CONUS zone. And again this is much higher in comparison to the WAAS alert figure for the same date and time.

We should emphasize that much better agreement between WAAS alert figure, real positioning and modelling data was achieved for the event on February 15th, 2011 in comparison to the one on June 22nd, 2015. It probably proves that the WAAS algorithm reacts better on the system outages events (see Table 2) than on geomagnetic storm, especially under high-latitude ionosphere environment. In our opinion such disagreement between the WAAS alert figure and our computation results can be caused by multi-scale ionospheric irregularities which are generated in the period of geomagnetic storm and can disrupt the correct GIVE values computations.

Based on the long time previous results it has been accepted that geomagnetic storms bring increasing in intensity of all-scale disturbances of the ionospheric total electron content (TEC) within the Globe [17,18,19]. This idea was reflected in the GPS and WAAS ionospheric standard models which are in the base of GIVE value computations. Such approach however is not able to take into account the real multi-scale ionospheric disturbances. These disturbances mostly affect GNSS performance in local areas which are associated with the travelling pattern of the ionospheric irregular structure not only in high and low latitudes but also in mid-latitudes.

In spite of the mid-latitude ionosphere usually does not contain the sources to generate significant multi-scale ionospheric disturbances both the equatorial and the polar areas can bring ones into the mid- latitudes especially under magnetic storm conditions [20-22]. Low-latitude ionosphere contents specific ionospheric disturbances which are known as “ionospheric super-bubble”. These “bubbles” can penetrate in mid-latitudes up to 35-37°N under geomagnetic storm conditions [21]. On the other hand polar ionosphere can be a source of strong large-scale travelling ionospheric disturbances which are generated within the pulsing boarder of the auroral oval area and propagate toward the mid-latitudes as well [7].

Analyzing the ionospheric effects of numerous of magnetic storms in a period from 2000 to 2004 it was found that a region with intense with multi-scale electron density irregularities emerges during magnetic storms on the border of the auroral oval. The region of increased in-

tensity of these irregularities can have a large spatial scale (hundreds and thousands kilometers) and travel following the uniformly moving or pulsating auroral oval border<sup>[7]</sup>. The instantaneous pattern of ionospheric irregularities distribution is heterogeneous in space and rapidly changes in time. It means that we must not expect global concurrent effect of the geomagnetic disturbances in GNSS and WAAS performance. It is more likely that the geomagnetic storm effects bring local sharp positioning quality deterioration. It can happen suddenly anytime not only within the main phase of geomagnetic storm but also within during its recovering phase.

All the above mentioned probably tells that it is necessary to revise the main WAAS building concept taking into account the latitudinal features of the ionosphere. The main concept of the WAAS integrity monitoring is that the confidence bounds of expected ranging errors must be large enough to describe the error in the correction, but tight enough to allow the operation to proceed. If it is not possible to distinguish between nominal and disturbed conditions, then we must always assume disturbed conditions are present. As we could see earlier this concept may get false alarm.

In case the main concept of the WAAS integrity monitoring has to stay the same, there are two main ideas to solve the above mentioned contradiction. Firstly, we can find a solution to detect ionospheric irregularities so that we can provide a high level of service during undisturbed time periods<sup>[23,24]</sup>. A reduced level of expected service would only be necessary during periods of detected ionospheric disturbances<sup>[23]</sup>. In order to realize this solution in practice the detection scheme of the ionospheric disturbances must be extremely robust, in order to provide the necessary level of protection. The integrity requirements for precision approach guidance set the probability of hazardously misleading information below  $10^{-7}$  per approach. Therefore, the chance of an undetected ionospheric irregularity must be at a similarly small level. Taking into account the above mentioned, it is unlikely to achieve such high probability of undetected multi-scale ionospheric disturbances even in mid-latitudes let alone high and low latitude areas.

Secondly, WAAS can also be modernized to take advantage of new signals of all global positioning systems (GLONASS, BeiDou, GALILEO, QZSS etc) and GEOs. Indeed by only upgrading the WAAS Reference Station (WRS) receivers to measure Galileo signals we can double our sampling of the ionosphere. The increased sampling translates into smaller broadcast confidence values on the single frequency ionospheric corrections. These lower values lead to higher availability. Similarly, the

L5 signal has better noise properties and can be acquired at a lower elevation angle. This leads less uncertainty in the ionospheric measurements and to smaller confidence bounds as well<sup>[25]</sup>. In reality, however, serious unpredicted obstacles were unfolded in common multi-system signal data processing. GPS TEC measurements for the GIVE computation, although highly precise, are often rendered inaccurately due to satellite and receiver differential code biases (DCBs). Calculated satellite DCB values are now available from a variety of sources, but receiver DCBs generally remain an undertaking of the receiver operators and processing centers<sup>[26,27,28]</sup>.

The other serious problem here is comprised in significant difference in ranging errors accuracy from all current positioning system and another ranging data sources. For example, a consistent analysis of signal-in-space ranging errors (SISREs) was conducted for all current satellite navigation systems, considering both global average values and worst-user-location statistics. Global average SISRE values for the individual constellations amount to  $0.7 \pm 0.02$  m (GPS),  $1.5 \pm 0.1$  m (BeiDou),  $1.6 \pm 0.3$  m (Galileo),  $1.9 \pm 0.1$  m (GLONASS), and  $0.6 \pm 0.2$  m (QZSS) over a 12-month period in 2013/2014<sup>[27]</sup>.

Besides this we should take into account that some anomalies in particular SV ranging are also possible. As an example of it GPS satellite oscillator anomalies mimicking ionospheric phase scintillation can be pointed out. Such ranging anomalies can be expected from an anomaly in the satellite's oscillators which are a persistent phenomenon. They have the potential to generate false alarms in the systems to forewarn of GPS outages due to the ionospheric scintillation<sup>[29,30]</sup>.

And finally, the capability of GNSS receivers to track multiple GNSS signals poses the problem of mutual alignments of reference frames and time scales<sup>[31]</sup>. System biases should possibly be computed in advance and made known to the user, so that the only unknowns for code point positioning are the receiver coordinates and the receiver clock offset relative to a unique time scale<sup>[28]</sup>.

In our opinion in order to achieve high confidence of WAAS positioning availability alerts real ionospheric measurements within the wide area coverage zone must be involved instead of the WAAS GIVE values<sup>[33]</sup>. The better way to realize this idea is to combine the WAAS and LAAS solutions. According to<sup>[12]</sup> in order to form the ranging confidence bounds the real ranging which were collected from WRSs in WAAS coverage zone are decomposed as following

$$\sigma_{TOT}^2 = \sigma_{flt}^2 + \sigma_{UIRE}^2 + \sigma_{air}^2 + \sigma_{trop}^2 \quad (7)$$

These terms correspond to: the satellite clock and ephemeris corrections error ( $\sigma_{fit}$ ), the ionospheric correction error ( $\sigma_{UIRE}$ ), the code noise, multipath error ( $\sigma_{air}$ ), and the troposphere error ( $\sigma_{trop}$ ).

According to their impact on the final UDRE and GIVE values we can divide these errors into two groups: 1) the global ranging correction errors which do not depend on the user's location within WAAS coverage zone and 2) the locally dependent ranging correction errors which are strictly dependent on the user's position within WAAS coverage zone. The first group of the errors contains the satellite clock and ephemeris corrections error ( $\sigma_{fit}$ ) as well as differential code biases for SVs and the second group shell include tropospheric, ionospheric and multipath errors.

WAAS can provide high confident corrections and integrity monitoring for the first group ranging errors within the coverage zone in any geophysical environment. On the other hand the  $\sigma_{UIRE}$ ,  $\sigma_{air}$  and  $\sigma_{trop}$  components are strictly dependent on the local environment of radio wave propagation. There are a numerous research which proves low confidence of locally dependent ranging corrections under geomagnetic storms, solar radio flares and another irregular external impacts. Probably it means that better solution is to get these ranging error statistics not from WAAS output but from the local GNSS-sites output. Today there are several types of such local GNSS networks which can be considered to involve in the above mentioned implementation: Geodynamics and geophysical services network, like GEONET, IGS, RTK-networks; Local Area DGPS; the WAAS WRSs sites etc.

The  $\sigma_{UIRE}$ ,  $\sigma_{air}$  and  $\sigma_{trop}$  statistics can be collected at the above mentioned local GNSS sites and broadcast to the nearest users within a local coverage zone. Combining "global" ranging correction with locally dependent ranging corrections the user equipment can use both WAAS and Local network ranging data statistics to compute correspondent HPL (VPL) with higher confidence.

**Acknowledgments:** This work is supported by the Chinese Academy of Sciences (CAS) program of "Light of West China" (Grant No. 29Y607YR000103), Chinese Academy of Sciences, Russia and Ukraine and other countries of special funds for scientific and technological cooperation (Grant No. 2BY711HZ000101) and the Russian Science Foundation Grant No. 17-77-20005. The second author is financially supported by the China Scholarship Council (CSC) for his visiting postdoctoral research at the German Research Centre for Geosciences (GFZ).

## References

- [ 1 ] Global positioning system wide area augmentation system (WAAS) performance standard (2008). Appendix B, 1st Edition
- [ 2 ] Tossaint M, Samson J, Toran F, Ventura-Traveset J, Hernandez-Pajares M, Juan JM, Sanz J, Ramos-Bosch P (2007), "The Stanford—ESA integrity diagram: a new tool for the user domain SBAS integrity assessment", *Navigation*, Institute of Navigation, 2(54), 153–162. <https://doi.org/10.1002/j.2161-4296.2007.tb00401.x>
- [ 3 ] Datta-Barua S, Lee J, Pullen S, Luo M, Ene A, Qiu D, Zhang G, Enge P (2010), "Ionospheric threat parameterization for local area Global-Positioning-System-based aircraft landing systems", *J Aircraft*, 47(4), 1141–1151. <https://doi.org/10.2514/1.46719>
- [ 4 ] Kintner PM, Kil H, and E. de Paula (2001), "Fading Time Scales Associated with GPS Signals and Potential Consequences", *Radio Science*, 36(4), 731–743. <https://doi.org/10.1029/1999RS002310>
- [ 5 ] Paulo L, Fortes S, Lin T, and Lachapelle G (2015), "Effects of the 2012–2013 solar maximum on GNSS signals in Brazil", *GPS Solutions*, 19, 309–319. [doi.org/10.1007/s10291-014-0389-1](https://doi.org/10.1007/s10291-014-0389-1)
- [ 6 ] Sieradzki R and Paziewski J (2016), "Study on reliable GNSS positioning with intense TEC fluctuations at high latitudes", *GPS Solutions*, 20, 553–563. <https://doi.org/10.1007/s10291-015-0466-0>
- [ 7 ] Afraimovich EL, Astafyeva EI, Demyanov VV, and Gamayunov IF (2009), "Mid-latitude amplitude scintillation of GPS signals and GPS performance slips", *Advances in Space Research*, 43, 964–972. <https://doi.org/10.1016/j.asr.2008.09.015>
- [ 8 ] Wide-area augmentation system performance analysis report, Report #36. Reporting Period: January 1 to March 31, 2011. Available from: <http://www.nstb.tc.faa.gov/DisplayArchive.htm>
- [ 9 ] Wide-area augmentation system performance analysis report, Report #53. Reporting Period: April 1 to June 30, 2015. Available from: <http://www.nstb.tc.faa.gov/DisplayArchive.htm>
- [10] Estey L. and Meertens C (1999), "TEQC: The Multi-Purpose Toolkit for GPS/GLONASS Data", *GPS Solutions*, 3(1), 42-49. <https://doi.org/10.1007/PL00012778>
- [11] SARPS Amendment 77, Annex 10 to the Convention on International Civil Aviation, Aeronautical Telecommunications: International Standards and Recommended Practices, Volume 1, Radio Navigation Aids, November 2002
- [12] Minimum Operation Performance Standard: MOPS

- DO-229C. Version C, Appendix A: Wade Area Augmentation System Signal Specification, 2001 RTCA Inc.
- [13] Mylnikova AA, Yasyukevich YV, Kunitsyn VE, and Padokhin AM (2015), “Variability of GPS/GLONASS differential code biases”, *Results in Physics*, 5, 9–10. <https://doi.org/10.1016/j.rinp.2014.11.002>
- [14] Schaer S (2012), “Overview of GNSS biases. International GNSS Service. Workshop on GNSS Biases”. [Electronic resource]. URL: [http://www.biasws2012.unibe.ch/pdf/bws12\\_1.3.1.pdf](http://www.biasws2012.unibe.ch/pdf/bws12_1.3.1.pdf)
- [15] Hilla S, and Cline M (2004), “Evaluating pseudorange multipath effects at stations in the National CORS Network”, *GPS Solutions*, 7, 253–267. <https://doi.org/10.1007/s10291-003-0073-3>
- [16] Xia L (2004), “Multipath in GPS navigation and positioning”, *GPS Solutions*, 8, 49–50. <https://doi.org/10.1007/s10291-004-0085-7>
- [17] Lekshmi DV, Balan N, Ram ST, and Liu JY (2011), “Statistics of geomagnetic storms and ionospheric storms at low and mid latitudes in two solar cycles”, *Journal of Geophysical Research*, 116, A11328. <https://doi.org/10.1029/2011JA017042>
- [18] Jakowski N, Mayer C, Wilken V, Borries C, and Doherty PH (2007), “Ionosphere Storms at High and Mid-latitudes Monitored by Ground and Space Based GPS Techniques”, *Proceedings of the International Beacon Satellite Symposium*, Boston College, June 11–15, Boston, USA
- [19] Aarons J, Mullen JP, Whitney H. [et al.] (1981), “VHF Scintillation Activity Over Polar Latitudes”, *Geophysical. Res. Lett.*, 8, 277–280. <https://doi.org/10.1029/GL008i003p00277>
- [20] Afraimovich EL, Astafieva EI, Demyanov VV (2004), “Ionosphere Geomagnetic Variations and GPS Positioning Errors During the Major Magnetic Storm on 29–31 October 2003”, *International Reference Ionosphere News*, 11 (3–4), 10–14
- [21] Demyanov VV, Yasyukevich YV, Ishin AB, and Astafyeva EI (2012), “Effects of ionosphere super-bubble on the GPS positioning performance depending on the orientation relative to geomagnetic field”, *GPS Solutions*, 16, 181–189. <https://doi.org/10.1007/s10291-011-0217-9>
- [22] Veetil SV, Haralambous H, and Aquino M (2017), “Observations of quiet-time moderate mid latitude L-band scintillation in association with plasma bubbles”, *GPS Solutions*, 21, 1113–1124. <https://doi.org/10.1007/s10291-016-0598-x>
- [23] Walter T, Blanch J, and Rife J (2004), “Treatment of Biased Error Distributions in SBAS”, Presented at the International Symposium on GNSS/GPS, December, 2004, Sydney, Australia [Electronic resource]. – Stanford, 2004. URL: [http://web.stanford.edu/group/scpnt/gpslab/pubs/papers/Walter\\_ISGNSS\\_2004.pdf](http://web.stanford.edu/group/scpnt/gpslab/pubs/papers/Walter_ISGNSS_2004.pdf)
- [24] Rife J, Walter T, and Blanch J (2004), “An Overbounding SBAS and GBAS Error Distributions with Excess-Mass Functions”, Presented at the International Symposium on GNSS/GPS, December, 2004, Sydney, Australia [Electronic resource]. – Stanford, 2004. URL: [http://web.stanford.edu/group/scpnt/gpslab/pubs/papers/Rife\\_IGNSS\\_2004.pdf](http://web.stanford.edu/group/scpnt/gpslab/pubs/papers/Rife_IGNSS_2004.pdf)
- [25] Walter T, Enge P, Reddan P (2004), “Modernizing WAAS”, Presented at the International Symposium on GNSS/GPS, December, 2004, Sydney, Australia [Electronic resource]. – Stanford, 2004. URL: [http://web.stanford.edu/group/scpnt/gpslab/pubs/papers/Walter\\_IONGNSS\\_2004.pdf](http://web.stanford.edu/group/scpnt/gpslab/pubs/papers/Walter_IONGNSS_2004.pdf)
- [26] El-Mowafy A (2014a), “GNSS Multi-Frequency Receiver Single-Satellite Measurement Validation Method”, *GPS Solutions*, 18(4), 553–561. <https://doi.org/10.1007/s10291-013-0352-6>
- [27] Montenbruck O, Steigenberger P and Hauschild A (2015), “Broadcast versus precise ephemerides: a multi-GNSS perspective”, *GPS Solutions*, 19, 321–333. <https://doi.org/10.1007/s10291-014-0390-8>
- [28] Hakansson M, Jensen ABO, Horemuz M, and Hedling G (2017), “Review of code and phase biases in multi-GNSS positioning”, *GPS Solutions*, 21, 849–860. <https://doi.org/10.1007/s10291-016-0572-7>
- [30] Benton CJ, and Mitchell CN (2012), “GPS satellite oscillator faults mimicking ionospheric phase scintillation”, *GPS Solutions*, 16, 477–482. <https://doi.org/10.1007/s10291-011-0247-3>
- [31] Benton CJ, and Mitchell CN (2014), “Further observations of GPS satellite oscillator anomalies mimicking ionospheric phase scintillation”, *GPS Solutions*, 18, 387–391. <https://doi.org/10.1007/s10291-013-0338-4>
- [32] El-Mowafy A (2014b), “GNSS multi-frequency receiver single-satellite measurement validation method”, *GPS Solutions*, 18, 553–564 <https://doi.org/10.1007/s10291-013-0352-6>
- [33] Demyanov VV, and Likhota RV (2015), “The method of GNSS positioning availability control for transportation applications”, *Machines, Technologies, Materials*, 5, 11–13. ISSN 1313-0226